Prediction of Off-Runway Takeoff and Landing Performance

A. J. KUCHINKA*
Lockheed-Georgia Company, Marietta, Ga.

Theoretical equations are presented for the determination of static and dynamic soil forces against a pneumatic tire. The equations are applicable to any pneumatic tire, inflated to any reasonable pressure, which is being pulled or pushed across an arbitrary soil. The equations require that the soil properties k_c, k_ϕ, and n must be known. Particular application is made to the prediction of aircraft take-off and landing ground roll distances. Correlation of calculated vs measured distance is shown for both landing and takeoff.

Nomenclature

A = area, in.^{2}
a = acceleration, ft/sec^2
BQ = brake torque, ft-lb
b = footprint tire width, in.
D = aerodynamic drag, lb
dA = differential of A
$d\mathbf{F}_s$ = differential of $\mathbf{F}_s$
$d\theta'$ = differential of θ'
$\mathbf{F}_{dx}$ = dynamic force in the x direction, lb
$\mathbf{F}_{dz}$ = dynamic force in the z direction, lb
F_{mx} = main gear force in the x direction, lb
F_{mz} = main gear force in the z direction, lb
F_{nx} = nose gear force in the x direction, lb
F_{nz} = nose gear force in the z direction, lb
$\mathbf{F}_s$ = static force, lb
$\mathbf{F}_{sx}$ = static force in the x direction, lb
$\mathbf{F}_{sz}$ = static force in the z direction, lb
i, j, k, n = unit vectors
K = braking effectiveness factor
k_c = physical soil value associated with sinkage, lb/in.$^{n+1}$
k_ϕ = physical soil value associated with sinkage, lb/in.$^{n+2}$
k_1, k_2, k_3, k_4 = lengths that are constants for a given configuration, in.
L = aerodynamic lift, lb
M_y = aerodynamic pitching moment about c.g., in.-lb
m = aircraft mass, slugs
N_m = number of main gear tires
N_n = number of nose gear tires
n = exponent of sinkage
p = pressure, psi
p_c = carcass stiffness represented as an equivalent pressure, psi
p_g = ground pressure, psi
p_i = tire inflation pressure, psi
r = tire radius, in.
slope = runway slope, rad
T = aircraft thrust, lb
$\mathbf{V}_{cr}$ = critical velocity above which the sum of the static and dynamic pressure is equal to the sum of the inflation and carcass pressures, knots
$\mathbf{V}_g$ = aircraft ground velocity, knots
$\mathbf{V}_n$ = velocity normal to tire surface at point P on the periphery of the tire, knots
$\mathbf{V}_p$ = velocity of point P on the periphery of the tire, knots
W = aircraft gross weight, lb
Z_o = sinkage depth of static tire, in.
$\Delta\theta$ = angle subtended by Z_o, rad
$\Delta\theta_1$ = angle defined by Fig. 4, rad
$\Delta\theta_2$ = angle defined by Fig. 4, rad
θ = half-angle subtended by tire "flat" spot, rad
θ' = variable of integration, rad
μ_r = rolling coefficient of friction
μ_b = braking coefficient of friction
ρ = soil density, slugs/ft^3

Presented as Preprint 65-328 at the AIAA Second Annual Meeting, San Francisco, Calif., July 26–29, 1965; submitted August 6, 1965; revision received January 3, 1966.

* Aircraft Development Engineer, Specialist.

Introduction

THE retarding force produced by soils on aircraft undercarriages plays an important part in determining takeoff and landing performance when aircraft operation is from unprepared fields. The soil retarding force can be of sufficient magnitude to prevent takeoffs or cause structural failure during landings for conditions where hard-surface operations normally would be safe and possible. The Lockheed-Georgia Company is extremely interested in the assault capabilities of aircraft. The prediction of soil retarding forces is not only vital to estimating performance but also is a vital part of optimizing assault techniques and finding improvements in tire design and servicing for specific applications.

Lockheed-Georgia Company has conducted takeoff and landing tests on sand, sod, and clay fields. An attempt to determine soil retarding forces by the simple expediency of subtracting on-runway data from off-runway data met with little success. This resulted in the necessity of finding a theoretical means of determining soil retarding forces.

A survey of available literature reveals that soil mechanics is a relatively new field. For many years the construction industry relied upon rules of thumb and prior experience to determine soil compaction requirements. In recent years the primary emphasis has been on the development of empirical formulas to determine the relationships between soils and objects in contact with soil. Various individuals have made significant contributions to the field of soil mechanics (theoretical development); but to the best of the author's knowledge, personnel at the Land Locomotion Laboratory in Centerline, Michigan seem to have developed a major portion of recent theoretical and empirical formulas concerning reactions between soils and tracks or wheels transversing the soils.

Theoretical Development

Static Considerations

Consider a pneumatic tire moving at very low speed (essentially static) over a soft, homogeneous soil as shown in Fig. 1. The tire sinks into the soil to depth Z_o at which point the soil pressure causes the tire to flatten out. The flat spot subtends the angle 2θ; the arc of tire sunk into the soil subtends angle $\Delta\theta$. The tire is of radius r, width b, carries the load $\mathbf{F}_{sz}$, and is moved along by horizontal force $\mathbf{F}_{sx}$. The resultant force is $\mathbf{F}_s$. The distributed load diagram represents the soil pressure distribution (denoted by p_g) against the tire. Note that p_g is a scalar but is shown acting normal to the tire surface. Then

$$-\mathbf{F}_s = \int_A p_g \mathbf{n}\, dA \qquad (1)$$

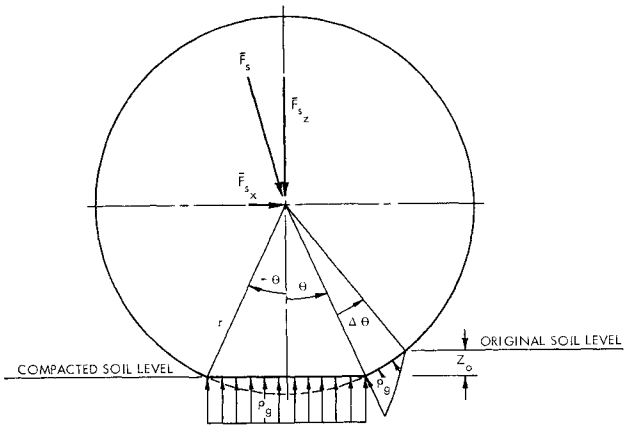

Fig. 1 Static diagram.

where boldface letters indicate the value is a vector, as opposed to a scalar. The vector $\mathbf{n}$ is a unit vector normal to the surface. Now introduce the empirical equation proposed by Bekker[1,2] of the Land Locomotion Laboratory which expresses ground pressure as a function of the soil parameters k_c, k_ϕ, and n

$$p_g = (k_\phi + k_c/b)\, Z^n \tag{2}$$

Equation (2) expresses the pressure distribution on the arc of tire below the soil surface, and

$$p_g = p_i + p_c \tag{3}$$

gives the pressure on the flat portion. The term p_c represents the stiffness of the tire carcass as an equivalent pressure distribution. Values for p_c are a function of tire construction and inflation pressure; they should be determined experimentally or from data supplied by the tire manufacturer.

The terms dA and $\mathbf{n}$ similarly may be defined in two parts. Over the arc of the tire $dA = rb\, d\theta'$ and $\mathbf{n} = \sin\theta'\,\mathbf{i} + \cos\theta'\,\mathbf{k}$. Combining the two terms gives

$$\mathbf{n}\, dA = rb(\sin\theta'\, d\theta'\,\mathbf{i} + \cos\theta'\, d\theta'\,\mathbf{k}) \tag{4}$$

where the prime (′) indicates the variable of integration. In Eq. (4), θ' will vary from θ to $\theta + \Delta\theta$. The expression

$$\mathbf{n}\, dA = rb\cos\theta'\, d\theta'\,\mathbf{k} \tag{5}$$

applies to the flat portion of the tire surface, and θ varies from $-\theta$ to θ. The sink depth Z obviously may be written as

$$Z = r[\cos\theta' - \cos(\theta + \Delta\theta)] \tag{6}$$

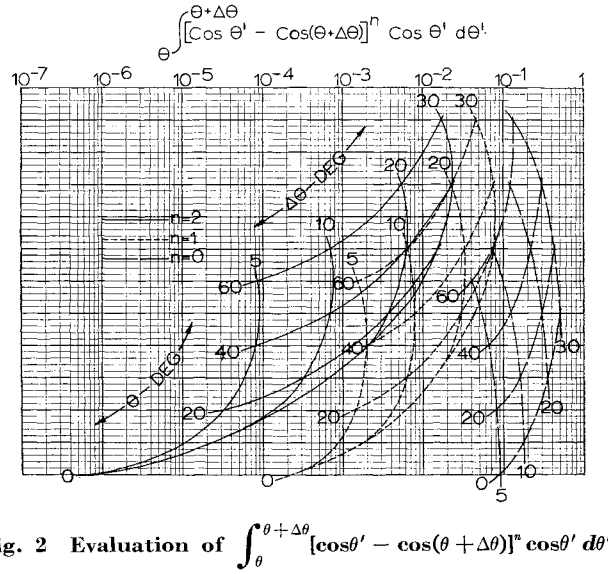

Fig. 2 Evaluation of $\int_{\theta}^{\theta+\Delta\theta} [\cos\theta' - \cos(\theta+\Delta\theta)]^n \cos\theta'\, d\theta'$.

Thus,

$$dZ = -r\sin\theta'\, d\theta' \tag{7}$$

Substitution of Eqs. (2–7) into Eq. (1) yields

$$-\mathbf{F}_s = \int_{-\theta}^{\theta} (p_i + p_c) rb\cos\theta'\, d\theta'\,\mathbf{k} + \int_{\theta}^{\theta+\Delta\theta} \left(k_\phi + \frac{k_c}{b}\right) r^n[\cos\theta' - \cos(\theta+\Delta\theta)]^n\, rb\cos\theta'\, d\theta'\,\mathbf{k} + \int_{\theta'=\theta}^{\theta'=\theta+\Delta\theta} \left(k_\phi + \frac{k_c}{b}\right)[Z(\theta')]^n\, b[-dZ(\theta')]\mathbf{i}$$

where $Z(\theta')$ denotes that Z is a function of θ'. The next logical step is to separate $\mathbf{F}_s$ into its two components, $\mathbf{F}_{s_x}$ and $\mathbf{F}_{s_z}$, and perform the integration. Thus,

$$-\mathbf{F}_{s_x} = [(k_c + bk_\phi)/(n+1)](Z_0)^{n+1}\,\mathbf{i} \tag{8}$$

and

$$-\mathbf{F}_{s_z} = 2(p_i + p_c) rb\sin\theta\,\mathbf{k} + \left(k_\phi + \frac{k_c}{b}\right) r^{n+1} b\mathbf{k} \int_{\theta}^{\theta+\Delta\theta} [\cos\theta' - \cos(\theta+\Delta\theta)]^n \cos\theta'\, d\theta' \tag{9}$$

Equation (8) is recognizable as the soil compaction resistance equation presented in Ref. 1. Equation (9) contains the term

$$\int_{\theta}^{\theta+\Delta\theta} [\cos\theta' - \cos(\theta+\Delta\theta)]^n \cos\theta'\, d\theta'$$

which cannot be integrated (from the pure mathematical sense) for all arbitrary values of n. Digital computers and numerical integration can be used to overcome this obstacle.

If a digital computer is not available, the carpet plot presented in Fig. 2 may be used to perform the evaluation. Note that the term has continuous derivatives over the practical range of n values from 0 through 2, and that the term may be integrated in closed form for integer values of n. This means the solution of the integral must be smooth and continuous and will not contain an inflection point (because the third derivative is continuous). The evaluation was performed for n values of 0, 1, and 2 over a range of θ and $\Delta\theta$ values. The results are plotted in carpet form on semilog paper in Fig. 2. It is believed that linear interpolation for noninteger n values will yield sufficiently accurate results. If an individual wishes to use the preceding technique and desires better accuracy than is possible with linear interpolation, the term may be integrated for higher values of n. A smooth continuous curve may then be drawn through all of the points and the integral evaluation read from the curve.

Dynamic Considerations

Now consider the pneumatic tire moving at relatively high speed. The external forces acting upon the tire will include the static forces previously mentioned and certain dynamic forces. In Fig. 3 point 0 is the instantaneous center of rotation, and point P is a point on the periphery of the tire moving with velocity $\mathbf{V}_p$ with respect to the soil. The tire is rolling along the ground with velocity $\mathbf{V}_g$. Now assume the soil is an inviscid fluid and that the classic term $\mu_r\mathbf{F}_z$ will account for the shearing stress between the tire and the soil. Then the only component of $\mathbf{V}_p$ which results in exerting dynamic pressure against the tire surface is $\mathbf{V}_n$, where

$$\mathbf{V}_n = \mathbf{V}_g\sin\theta' \tag{10}$$

Then the incremental force $d\mathbf{F}_d$ exerted by the dynamic pressure on tire surface dA is given by

$$d\mathbf{F}_d = p\,\mathbf{n}\, dA = \tfrac{1}{2}\rho(1.69)^2(\mathbf{V}_n\cdot\mathbf{V}_n)\mathbf{n}(dA/144) \tag{11}$$

Substituting Eqs. (4) and (10) into Eq. (11), integrating, and separating the total dynamic force into its two components gives

$$\mathbf{F}_{d_x} = \tfrac{1}{288}\rho(1.69\ V_g)^2 rb\ \mathbf{i}\{\tfrac{1}{3}[\cos^3(\theta+\Delta\theta) - \cos^3\theta] - \cos(\theta+\Delta\theta) + \cos\theta\} \quad (12)$$

$$\mathbf{F}_{d_z} = \tfrac{1}{288}\rho(1.69\ V_g)^2 rb\ \mathbf{k}\ \tfrac{1}{3}[\sin^3(\theta+\Delta\theta) - \sin^3\theta] \quad (13)$$

Equations (8) and (12) cannot always be added to get the total horizontal force, nor will (9) and (13) always yield the vertical load. This is because the equations do not impose a limit on the pressure distribution. To explain, consider the case where the horizontal velocity is great enough that everywhere on the wheel the sum of the static and dynamic pressures would equal or exceed $p_i + p_c$. (For future reference, define this situation as $\mathbf{V}_g \geqq \mathbf{V}_{cr}$.) Obviously the sum of static and dynamic pressure cannot exceed $p_i + p_c$. This limit will not be exceeded because the dynamic pressure will decrease; that is, the tire will deflect inward with velocity sufficient to insure that the total pressure just equals $p_i + p_c$. Therefore, when $\mathbf{V}_g \geqq \mathbf{V}_{cr}$, the total horizontal and vertical forces are given by

$$\mathbf{F}_x = (p_i + p_c)rb[\cos\theta - \cos(\theta+\Delta\theta)]\mathbf{i} \quad (14)$$

and

$$\mathbf{F}_z = (p_i + p_c)\ rb\ [\sin(\theta+\Delta\theta) + \sin\theta]\mathbf{k} \quad (15)$$

Thus, the ideal situation is to write a set of equations that describe the forces for any and all conditions.

General Equation

In Fig. 4 the arc of tire is shown flat to better demonstrate the pressure distribution situation. The condition depicted is that $\mathbf{V}_g$ is less than but sufficiently close to $\mathbf{V}_{cr}$ so that over two portions of the tire surface the total pressure is limited to $p_i + p_c$. The dotted lines indicate the magnitude the total pressure would assume if it were not limited. The general equation for pressure (ignoring limits) is

$$p = (k_\phi + k_c/b)r^n[\cos\theta' - \cos(\theta+\Delta\theta)]^n + \tfrac{1}{288}\rho(1.69V_g)^2\sin^2\theta' \quad (16)$$

Therefore, the points at which the pressure is limited may be found by trial and error solution of

$$p_i + p_c = (k_\phi + k_c/b)r^n[\cos(\theta+\Delta\theta_2) - \cos(\theta+\Delta\theta)]^n + \tfrac{1}{288}\rho(1.69V_g)^2\sin^2(\theta+\Delta\theta_2) \quad (17)$$

and

$$p_i + p_c = (k_\phi + k_c/b)r^n[\cos(\theta+\Delta\theta-\Delta\theta_1) - \cos(\theta+\Delta\theta)]^n + \tfrac{1}{288}\rho(1.69\ V_g)^2\sin^2(\theta+\Delta\theta-\Delta\theta_1) \quad (18)$$

between the limits of θ and $\theta + \Delta\theta$. Now please note. Evaluation of Eq. (17) is to be accomplished by increasing the value of $\Delta\theta_2$ until the right-hand side decreases to a value equal to the left-hand side. If a solution does not exist for $\Delta\theta_2 \leqq \Delta\theta$ the equation is indeterminate ($\mathbf{V}_g > \mathbf{V}_{cr}$). Evaluation of Eq. (18) is to be accomplished by first solving when $\Delta\theta_1 = 0$. If the right-hand side is equal to or less than $p_i + p_c$, then $\Delta\theta_1$ does equal zero. If the right-hand side is greater than $p_i + p_c$, increase $\Delta\theta_1$ until that side decreases to $p_i + p_c$. If a solution for $\Delta\theta_1 \leqq \Delta\theta$ does not exist, the equation is indeterminate.

A statement concerning these angle relationships seems appropriate at this time. When θ is nonzero, the angle $\Delta\theta$ is given by

$$\Delta\theta = \cos^{-1}(\cos\theta - Z_o/r) - \theta \quad (19)$$

Obviously θ is then the independent variable and $\Delta\theta$, $\Delta\theta_1$, and $\Delta\theta_2$ the dependent variables.

Now, when θ is zero, $\Delta\theta$ becomes the independent variable and $\Delta\theta_1$ and $\Delta\theta_2$ the dependent variables. In both cases

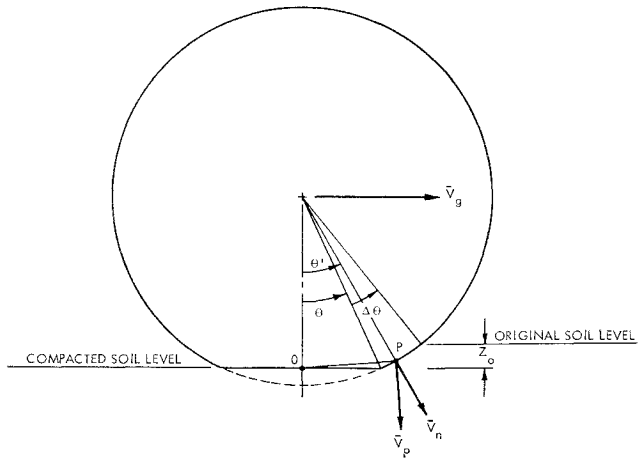

Fig. 3 Velocity diagram.

the independent variable must satisfy the condition that summation of all vertical forces is zero.

Equation (16) and the angle relationships defined by Eqs. (17) and (18) may be used to write the horizontal and vertical force equation as

$$\mathbf{F}_x = (p_i + p_c)rbi\int_\theta^{\theta+\Delta\theta_2}\sin\theta'\,d\theta' + (p_i + p_c)rbi\int_{\theta+\Delta\theta-\Delta\theta_1}^{\theta+\Delta\theta}\sin\theta'\,d\theta' + (k_\phi + k_c/b)bi\int_{\theta'=\theta+\Delta\theta-\Delta\theta_1}^{\theta'=\theta+\Delta\theta_2}[Z(\theta')]^n[-dZ(\theta')] + \tfrac{1}{288}\rho(1.69V_g)^2\,rbi\int_{\theta+\Delta\theta_2}^{\theta+\Delta\theta-\Delta\theta_1}\sin^3\theta'\,d\theta' \quad (20)$$

and

$$\mathbf{F}_z = (p_i + p_c)rb\mathbf{k}\int_{-\theta}^{\theta}\cos\theta'\,d\theta' + (p_i + p_c)\,rb\mathbf{k}\int_\theta^{\theta+\Delta\theta_2}\cos\theta'\,d\theta' + (p_i + p_c)\,rb\mathbf{k}\int_{\theta+\Delta\theta-\Delta\theta_1}^{\theta+\Delta\theta}\cos\theta'\,d\theta' + (k_\phi + k_c/b)r^{n+1}\,b\mathbf{k}\int_{\theta+\Delta\theta_2}^{\theta+\Delta\theta-\Delta\theta_1}[\cos\theta' - \cos(\theta+\Delta\theta)]^n \times \cos\theta'\,d\theta' + \tfrac{1}{288}\rho(1.69\ V_g)^2\,rb\mathbf{k} \times \int_{\theta+\Delta\theta_2}^{\theta+\Delta\theta-\Delta\theta_1}\sin^2\theta'\cos\theta'\,d\theta' \quad (21)$$

Integration of the equations in closed form (where possible) yields

$$\mathbf{F}_x = (p_i + p_c)rb[\cos\theta - \cos(\theta+\Delta\theta_2) + \cos(\theta+\Delta\theta-\Delta\theta_1) - \cos(\theta+\Delta\theta)]\mathbf{i} + (k_\phi + k_c/b)(br^{n+1}/n+1)[\cos(\theta+\Delta\theta_2) - \cos(\theta+\Delta\theta-\Delta\theta_1)]^{n+1}\,\mathbf{i} + (\rho rb/288) \times (1.69\ V_g)^2\{\tfrac{1}{3}[\cos^3(\theta+\Delta\theta-\Delta\theta_1) - \cos^3(\theta+\Delta\theta_2)] + \cos(\theta+\Delta\theta_2) - \cos(\theta+\Delta\theta-\Delta\theta_1)\}\mathbf{i} \quad (22)$$

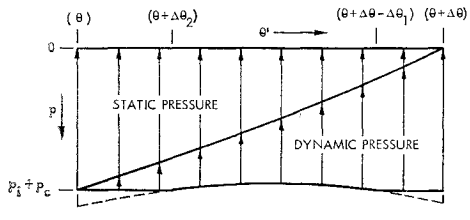

Fig. 4 Dynamic pressure limitation.

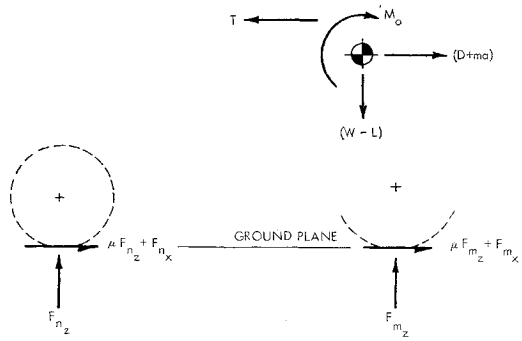

Fig. 5 Typical aircraft force and moment diagram.

and

$$\mathbf{F}_z = (p_i + p_c)\, rb\, [\sin\theta + \sin(\theta + \Delta\theta_2) + \sin(\theta + \Delta\theta) - \sin(\theta + \Delta\theta - \Delta\theta_1)]\mathbf{k} + (k_\phi + k_c/b)\, br^{n+1}\, \mathbf{k} \int_{\theta+\Delta\theta_2}^{\theta+\Delta\theta-\Delta\theta_1} [\cos\theta' - \cos(\theta + \Delta\theta)]^n \times \cos\theta'\, d\theta' + (\rho rb/288)(1.69\, V_g)^2\, \frac{1}{3}\, [\sin^3(\theta + \Delta\theta - \Delta\theta_1) - \sin^3(\theta + \Delta\theta_2)]\mathbf{k} \quad (23)$$

Equations (22) and (23) are then valid for any and all velocities when the following stipulation is observed. If Eqs. (17) and (18) are indeterminate ($\mathbf{V}_g \geqq \mathbf{V}_{cr}$), $\Delta\theta_2$ is to be set equal to $\Delta\theta$, and $\Delta\theta_1$ is to be set equal to zero. Equations (22) and (23) then will reduce to Eqs. (14) and (15).

Application to Aircraft

Takeoff Equations

The force equations in the previous section are completely general in nature. They may be applied to any pneumatic tire, inflated to any reasonable pressure, which is being pulled or pushed across an arbitrary soil. Now consider the force and moment diagram for a typical airplane moving along the ground as shown in Fig. 5. The main gear reaction (regardless of the number of struts) is assumed to act at one longitudinal location. The longitudinal equations of motion for this system may be written as

$$\Sigma F_x = T - D - \mu_r(W - L) - F_{n_x} - F_{m_x} - W(\text{slope}) = ma \quad (24)$$

$$\Sigma F_z = W - L - F_{n_z} - F_{m_z} = 0 \quad (25)$$

$$\Sigma M = M_0 + k_1 T + k_2(D + ma) + k_3(W - L) + k_4 F_{n_z} = 0 \quad (26)$$

where the summation of moments is taken about the intersection of the main gear reaction and the ground plane. Equations (24–26) are, in essence, static equations that have dynamic motion in the x direction only; that is, the aircraft pitching and vertical motions are constrained as nonexistent. The symbols k_1, k_2, k_3, and k_4 denote constants that are a function of the aircraft geometry. The aircraft thrust, drag, pitching moment, weight, and lift are assumed known as functions of aircraft velocity.

The three equations contain five unknowns; the nose gear (subscript n) and main gear (subscript m), horizontal and vertical forces, and the aircraft acceleration. However, the four forces may be determined by Eqs. (22) and (23) which contain only two unknown independent variables: θ (or $\Delta\theta$ if applicable) of the nose and main gear tires. The right-hand side of Eqs. (22) and (23) must be multiplied by N_n and N_m, the number of nose and main gear tires. The values of N_n and N_m may be adjusted to account for one tire rolling in the path of another.

Landing Equations

The landing equations differ from the takeoff equations by the addition of the braking term to Eq. (24). The equation may be written as

$$\Sigma F_x = T - D - \mu_r(W - L) - F_{n_x} - F_{m_x} - W(\text{slope}) - K[12(BQ)/r_m \cos\theta_m] = ma \quad (27)$$

where (BQ) denotes the braking torque applied, and K accounts for the loss in braking effectiveness due to brake cycling. The braking term and the rolling friction term could be combined to give

$$\Sigma F_x = T - D - K\mu_b(W - L) - F_{n_x} - F_{m_x} - W(\text{slope}) = ma \quad (28)$$

where μ_b is the braking coefficient of friction.

Solution Method

The methods by which the takeoff and landing equations may be solved are many and varied. The procedure used at Lockheed-Georgia Company is to express aircraft thrust, lift, drag, and pitching moment as functions of velocity and solve the longitudinal equations of motion to determine accelerations. Standard mathematical procedures are used to convert acceleration and velocities into ground roll distances. Rotation and air distances are computed by conventional techniques. Time lags or delays for reverse thrust and brake application are treated by conventional practices.

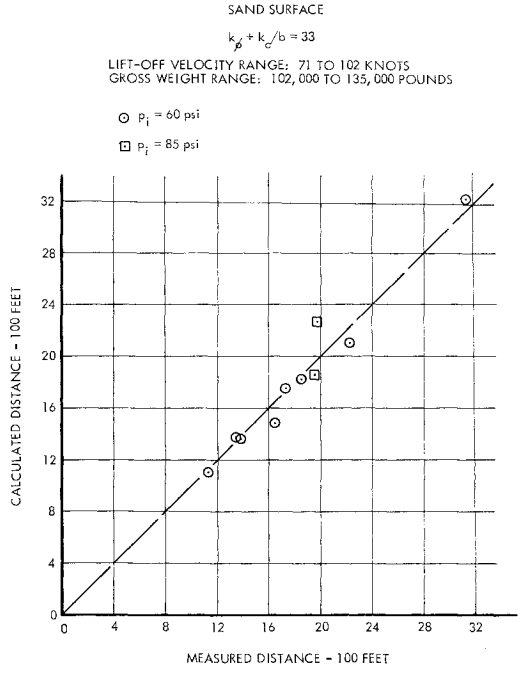

Fig. 6 Takeoff ground roll distance.

Table 1 Computed ground roll take off distance, feet, sand surface[a]

Gross weight condition	Sea level		4000 ft	
	With soil retarding forces	Without soil retarding forces	With soil retarding forces	Without soil retarding forces
Light	550	435	710	535
Low	905	690	1210	885
Medium	1440	1070	1930	1370
Heavy	2145	1550	3040	2040

[a] $k_\phi + k_c/b = 33$ $p_i = 60$ psi.

The unique solutions to the equations of motion are found by an iterative procedure. An arbitrary value of θ_m is selected initially and Eqs. (22) and (23) solved for the main gear horizontal and vertical forces. Equation (25) is then solved for the nose gear vertical force. The value of θ_n in Eq. (23) is then iterated upon until Eqs. (23) and (25) yield the same value for the nose gear vertical force. Equations (24) and (26) are then solved. If Eq. (26) yields a positive value, the original value of θ_m is too small. If the value is negative, the original value of θ_m is too large. If the value is zero, the solution is valid and the iterative process on θ_m is terminated.

Comparison with Flight Test

As mentioned in the introduction, the Lockheed-Georgia Company has conducted takeoff and landing tests on sand, sod, and clay fields. The composition of the sod and clay fields was such that no appreciable sinkage of the tires occurred. Actual rut depths for takeoffs and landings in the sand were not measured; however, taxi operations in sand produced 2-in. rut depths when the tires were inflated to 60 psi. Tire deflection tests show that for $p_i = 60$ psi, $p_c = 6$ psi. Reference 3 indicates that the sinkage exponent n for sand should be approximately 1.0. The preceding information and Eqs. (2) and (3) were used to get

$$k_\phi + k_c/b = 33 \tag{29}$$

This procedure is the only way the soil properties could be resolved since they were not measured during the tests. The aft main gear tires rolled in the path of the forward main gear tires; however, the value of N_m used in the equations equaled the number of main gear tires. This was based on a statement in Ref. 3 that test results indicate that rear wheels have the same motion resistance as front wheels.

A malfunction in a photographic timing device occurred during the sand tests which could not be detected until the film was developed. Unfortunately, the film was not available before completion of the tests. The ground roll distances for takeoffs and landings were good, but the aircraft velocities associated with lift-off and touch-down were inaccurate. Enough data were salvaged, however, to enable the following comparisons.

Takeoff Distance

Figure 6 shows a comparison between calculated and measured takeoff ground roll distances. The aircraft gross weight range is from 102,000 to 135,000 lb; the lift-off velocity varies from 71 to 102 knots. The circled data points represent takeoffs with tire inflation pressure set at 60 psi. A few takeoffs were made with 85-psi tire pressure and are depicted by the square symbols. The agreement in distances associated with two different tire pressures is indicative of the validity of the method of computation.

The effect of soil retarding forces of takeoff distance is not immediately obvious. Takeoff distance is inversely proportional to the excess thrust available. Conditions that reduce excess thrust (such as carrying external stores, high altitudes, and heavy gross weights) cause an increase in takeoff distance. Thus, the addition of soil retarding forces in some instances can reduce thrust to a level that will not permit takeoff. Soil retarding forces are a function of soil properties, gear geometry, and tire inflation pressure. It is necessary, therefore, to examine the actual conditions that prevail to determine their importance. Table 1 presents a comparison of calculated ground roll distances with and without soil retarding forces for the conditions which prevailed in Fig. 6. Data are presented for both sea level and 4000 ft standard day conditions to show the effect of altitude.

Table 2 Computed ground roll landing distance, feet, sand surface[a]

Gross weight condition	Sea level		4000 ft	
	With soil retarding forces	Without soil retarding forces	With soil retarding forces	Without soil retarding forces
Light	1060	1040	1200	1210
Low	1390	1460	1580	1690
Medium	1785	1960	2035	2300
Heavy	2210	2550	2525	3000

[a] $k_\phi + k_c/b = 33$ $\quad p_i = 60$ psi.

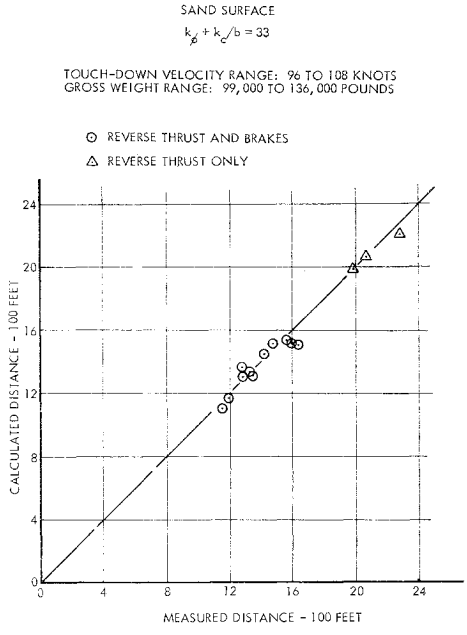

Fig. 7 Landing ground roll distance.

Landing Distance

Figure 7 shows a comparison between calculated and measured landing ground roll distances. The aircraft gross weight range is from 99,000 to 136,000 lb; the touch-down velocity varies from 96 to 108 knots. All landings shown were performed with a tire inflation pressure of 60 psi. The circled data points represent landings using both reverse thrust and brakes to decelerate the aircraft. Test data were used to determine that the value of K was 0.55. Three landings were made using only reverse thrust and are depicted by triangular symbols. Once again the correlation is deemed very good.

The effect of soil retarding forces on landing distance is not as pronounced as is the takeoff situation. In the landing case the aircraft is being decelerated. A loss in braking efficiency may or may not compensate for the soil retarding forces. Thus, the importance of including soil retarding forces in landing distance calculations depends on the importance of landing the maximum gross weight possible in a given field length. In the sod and the clay field tests, for example, the soil retarding forces were negligible. The loss in braking effectiveness, however, caused landing ground rolls to be about 100 ft longer than would be predicted for a hard-surface runway. Table 2 presents a comparison of calculated ground roll distances with and without soil retarding forces for the conditions that prevailed in Fig. 7. Data are presented for both sea level and 4000 ft standard day conditions to show the effect of altitude.

Conclusions

The method of predicting takeoff and landing ground roll distances for off-runway conditions agrees very well with

measured distances for flight data currently available to the author. However, additional test results for a wide variety of soils should be obtained before any general statements concerning the method are made.

References

[1] Bekker, M. G. and Janosi, Z., "Analysis of towed pneumatic tires moving on soft ground," Armed Services Technical Information Agency 256315(LL-62) (March 1960).

[2] "A soil value system for land locomotion mechanics," Department of the Army, Ordnance Tank-Automotive Command, Research & Development Div., Land Locomotion Research Branch Res. Rept. 5 (December 1958).

[3] Hanamoto, B., Liston, R. A., and Parker, C. B., "Terrain criteria in vehicle design," Land Locomotion Lab. Rept. 85 (June 1963).

MAY-JUNE 1966 J. AIRCRAFT VOL. 3, NO. 3

Torsional Oscillation of Helicopter Blades Due to Stall

NORMAN D. HAM*
Massachusetts Institute of Technology, Cambridge, Mass.

AND

MAURICE I. YOUNG†
The Boeing Company, Morton, Pa.

The amplitude of single degree of freedom torsional oscillations of highly loaded helicopter rotor blades is shown to be dependent on the blade mean pitch angle and the reduced frequency of the oscillation by experiments conducted in the static thrust condition. The origin of this torsional motion is indicated by consideration of the experimental chordwise pressure variation on a model helicopter blade during the stable limit cycle oscillation that occurs in the static thrust condition. The relationships between this torsional motion and the effective damping in pitch in the presence of stall are determined. The implications of these results in the forward flight condition are discussed qualitatively and illustrated by reference to flight test records. A simple numerical method of approximating the boundary of stable pitching-torsional oscillations in forward flight is described and a sample calculation shows good correlation with flight test results. The design problem is discussed briefly, and several refinements of blade planform are suggested as a potential means of avoiding the asymptotic rise in control loadings which now occur with contemporary design practice.

Nomenclature

b = section semichord, ft
k = section reduced frequency $\omega b/V$
x = nondimensional blade spanwise station
C_T = rotor thrust coefficient
I = pitching moment of inertia
ΔM = moment change at stall, ft/lb/ft
R = rotor radius, ft
V = section translational velocity, fps
α = section angle of attack
α_0 = section mean angle of attack
$\bar{\alpha}$ = amplitude of periodic angle of attack change
$\Delta\alpha_D$ = angle by which dynamic stall lags static stall
μ = rotor advance ratio $V/\Omega R$
ω = section angular frequency, rad/sec
ρ = air density, slugs/ft^3
σ = rotor solidity
θ = blade pitch angle
θ_0 = mean blade pitch angle
$\bar{\theta}$ = amplitude of periodic blade pitch change
ζ = damping ratio
$\bar{\zeta}$ = potential flow aerodynamic damping ratio
Ω = rotor rotational speed, rad/sec
$\Theta_1(x)$ = local fundamental torsion mode amplitude, rad

Subscript

θ = rotor blade pitching motion

Received May 20, 1965; revision received January 19, 1966. Presented at the Symposium on the Noise and Loading Actions on Helicopters, V/STOL Aircraft, and Ground Effect Machines, The Institute of Sound and Vibration Research, The University, Southampton, England, September 1965. This research was sponsored in part by the U.S. Army Research Office, Durham, North Carolina.

* Assistant Professor, Department of Aeronautics and Astronautics.

† Technology Manager, Advanced Technology, Vertol Division. Associate Fellow Member AIAA.

Introduction

ONE of the factors that can limit improvements in helicopter forward flight performance is a sharp increase in rotor torsional loads and vibration levels as appreciable portions of the rotor blades become stalled on the retreating side of the disk. Such regions of blade stalling that occur frequently in forward flight are shown below.

A previous investigation[1] indicated that one possible origin of increased torsional loading of rotor blades due to stall encountered in forward flight was a sharp decrease in the aerodynamic damping in pitch of the blades as they stalled. Other investigations of harmonically oscillating wings in forced motion[2-6] demonstrated that under stalled conditions the average damping in pitch over a cycle can become substantially negative and is strongly dependent on the wing mean angle of attack, the reduced frequency of the harmonic motion, the oscillation amplitude, and the airfoil configuration. Reference 3 indicated that the origin of the negative damping was aerodynamic moment hysteresis. Reference 2 applied the results of Ref. 3 to show that for certain mean angles of attack, reduced frequencies, and amplitudes of oscillation, the mean damping in pitch was zero over a cycle, and that, under these conditions, a self-excited but self-limiting one degree of freedom limit cycle oscillation of prescribed amplitude could occur.

Such oscillating motion, sometimes called stall flutter, is encountered in the highly loaded axisymmetric flow conditions of rotating machinery such as aircraft propellers or gas